Article

X-ray Exited Optical Luminescence of Eu in Diamond Crystals Synthesized at High-pressure High-temperature

Vasily T. Lebedev[1]*, Fedor .M. Shakhov[2], Alexandr Ya. Vul[2], Arcady A. Zakharov[1], Vladimir G. Zinoviev[1], Vera A. Orlova[3] and Eduard V. Fomin[1]

[1] B.P.Konstantinov Petersburg Nuclear Physics Institute, NRC Kurchatov Institute, 188300 Gatchina, Leningrad distr., Russia
[2] Ioffe Institute, Polytekhnicheskaya Street, 26, 194021 St. Petersburg, Russia
[3] V.G.Khlopin Radium Institute, 188300 Gatchina, Leningrad distr., Russia
*Correspondence: lebedev_vt@pnpi.nrcki.ru; +7(81371)46684

Abstract: Diamond powders with inclusions of europium atoms were synthesized at high pressure (7.7 GPa) and temperature (1800°C) from a mixture of pentaerythritol, $C(CH_2OH)_4$, and pyrolyzate of diphthalocyanine ($C_{64}H_{32}N_{16}Eu$) served as a special precursor. In prepared diamonds by X-ray fluorescence spectroscopy, we have found the concentration of Eu atoms of 51±5 ppm that is by two orders of magnitude greater than that in known natural and synthetic diamonds. X-ray diffraction, SEM, X-ray exited optical luminescence, Raman and IR spectroscopy have confirmed the formation of diamond monocrystals of high quality with embedded Eu atoms and a nitrogen content of ~500 ppm. Numerical simulation has allowed us determine the energy cost of 5.8 eV needed for the incorporation of a single Eu atom with adjacent vacancy into growing diamond crystal (528 carbons).

Keywords: diamond; synthesis; diphthalocyanine; pyrolyzate; lanthanide; X-ray; luminescence

1. Introduction

Problem of lanthanides (Ln) intercalation into the diamond lattice is relevant in fundamental and practical aspects and stimulates a search of ways of doping diamonds for various applications especially in optoelectronics and biomedicine owing to pronounced luminescent properties of embedded lanthanides when excited by UV, visible light or X-rays [1-3]. A successful solving of this problem will enable to produce really unique diamond crystals, which are unknown in nature.

Meanwhile, in tested fossil diamonds, the neutron activation analysis showed extremely low concentrations of lanthanides (~10^{-4} wt.%) localized in phosphate inclusions with a density close to that of diamond [4]. Authors [1] marked that usually the ion implantation to dope crystal with external elements irreversibly damages the host matrix, and this problem complicates a creation of the centers of luminescence in diamonds due to their graphitization in annealing process to restore the diamond structure.

Therefore, the authors [1] have developed an alternative method to incorporate europium into diamonds. They oxidized the surface of crystalline seeds (5 nm), then deposited on them a polyelectrolyte with linked chelate molecules containing Eu (III), and finally condensed carbon from gas phase on the samples (CVD method) [1]. Even so, the grown diamonds have had too low concentrations of Eu ions (~10^{-4} wt.%). The density functional modeling made it possible to simulate defects formation such as Eu atom in different charge states (3+ mainly) with attached 1–3 vacancies. The configuration with one vacancy turned out to be the most stable. In this case, a coordination sphere of 6 carbon atoms was formed around the Eu atom, and there were detected the electron transitions in Eu (III) involving f-orbitals [1].

To introduce Ln atoms into microcrystalline diamonds, detonation nanodiamond particles (~ 5 nm in size) were modified with Gd or Eu ions grafted to diamond surface through ion exchange with carboxyl groups. Then the samples were sintered at high

Preprints (www.preprints.org) | NOT PEER-REVIEWED | Posted: 6 December 2022 doi:10.20944/preprints202212.0085.v1

pressures and temperatures (7 GPa, 1300–1500°C, HPHT method) [3]. In these experiments, hydrocarbons and alcohols served instead of metal catalysts. In following energy-dispersive X-ray spectroscopy tests on the synthesized diamonds, the upper estimate of Ln amounts in diamonds was obtained ~0.01 at.%, while at the limit of the accuracy of measurements.

Authors [5] synthesized diamonds in the presence of Ln metallic inserts in the reactor (HPHT), but did not find in the obtained crystals any luminescence centers with a participation of Ln atoms. In addition to CVD and HPHT methods, the Ln embedding into diamonds has been performed by heat treatment (450; 700; 1000°C) of diamond powders impregnated with water-alcohol solutions of $Eu(NO_3)_3 \cdot H_2O$ [6]. In the samples it was detected an enhanced excitation of Eu^{3+} ions by UV radiation (280 nm) as compared to europium salt. This was explained by the appearance of Eu-O-C bonds through carboxyl groups at the diamond surface. However, in this case, there are no reasons to expect the intercalation of Ln atoms into the diamond lattice.

The cited works are relevant for biomedical tasks in theranostics, which is developing in the direction of using various nanostructures (quantum dots, metal or oxide particles, etc.) promising new functional abilities especially by X-ray activation. However, even in detailed review [7] it was not reported on the application of diamonds in this area. Mainly, this is explained by substantial difficulties of doping them with Ln and other metals. To date, no satisfactory solution has been found to the problem of introducing Ln into the diamond lattice. Meanwhile, this lattice is metastable at standard temperature and pressure and can be locally rearranged similarly to the formation of an interface with the $sp^3 \rightarrow sp^2$ transition in carbon orbitals as a result of the inclusion of large Ln atoms exceeding the lattice period.

However, heavy atom intercalation into diamond lattice needs substantial energies (14-17 eV for Eu^{3+} coupled with 1-3 vacancies in crystal fragment of 64 atoms) [1] because of most dense packing and strong interaction of carbons in diamond. Meanwhile, embedding highly fluorescent lanthanides into diamond lattice can be facilitated by the effect of atoms contraction with the increase of atomic number [8]. For instance, Tb has the atomic radius (r_{Tb} = 0.175 nm) by ~ 5 % less than that for Eu (r_{Eu} = 0.185 nm) when the atomic number is increased by ~ 3 % (Z_{Eu} = 63, Z_{Tb} = 65), and the difference $r_{Eu} - r_{Tb}$ = 0.010 nm is significant since it achieves ~14% of carbon atom radius (0.070 nm) [8]. Therefore, it seems a prospective way to use a series of Ln atoms with different atomic numbers for diamonds doping.

First, we started the studies with Eu and searched for effective precursors, in which single or few Eu atoms should be isolated inside durable carbon shells with a free volume suitable for the rearrangement of metal–carbon structures into diamond lattice under high pressures and temperatures (HPHT). Obviously, such objects as endometallofullerenes (EMF) could serve as promising candidates to be transformed into diamonds upon compression of molecular carbon shells placed around metal atoms. However, such experiments are still unknown due to very low availability of EMFs even in laboratory quantities.

As an alternative to EMF, we considered diphthalocyanines ($EuPc_2$). During pyrolysis in Ar atmosphere (900°C), such molecules, composed of two planar ligands connected by metal atom, lost mainly light elements (H, N). As a result, in a molecule the ligands with free bonds could be linked and a metal atom became closed in the carbon shell (~1 nm in size) [9]. We supposed also an encapsulation of few metal atoms in a common shell by combining several molecules into small globules forming porous matrix where the metal atoms are firmly kept and released only by heating above 1200°C when amorphous carbon transformed into graphite [9,10]. To convert Eu-containing pyrolyzates into diamonds, we have applied the HPHT method using also catalytic additive (pentaerythritol). First, we sought to find conditions for the formation of Eu-doped diamonds and to synthesize metal-enriched crystals. In the following experiments, we determined the Eu content in diamonds and studied their structure and physicochemical properties, as well as simulating the growth of crystals with the incorporation of Eu into the diamond lattice.

Preprints (www.preprints.org) | NOT PEER-REVIEWED | Posted: 6 December 2022 doi:10.20944/preprints202212.0085.v1

2. Experimental

2.1. Materials

Doped diamonds were synthesized using special precursors being the carbon matrices with encapsulated Eu atoms. These materials, pyrolyzates with composition EuC_X (X ~ 30–40), we prepared from diphthalocyanines ($EuPc_2$) [9,11] in which molecules the planar $C_{32}H_{16}N_8$ ligands (Pc) are firmly linked through a metal atom (M = Eu) (Figure 1).

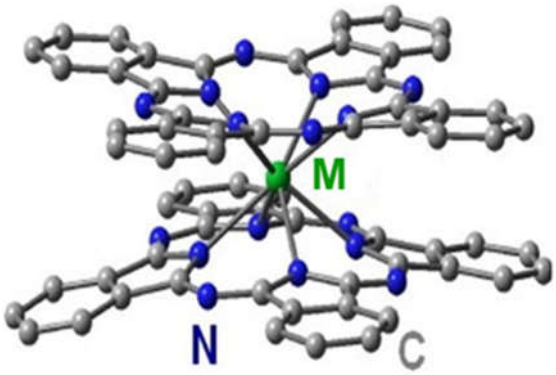

Figure 1. Diphthalocyanine molecule with a metal atom (M = Eu) linking organic ligands.

First, for the synthesis of the $LnPc_2$, the organic component, o-phthalonitrile, was placed into a quartz reactor and washed with argon flow [9]. At a constant passage of argon (~0.5 l/min), the temperature in the reactor was raised to 220–250°C. Then the salt (Eu acetate) was added in a mass ratio of 1:6 to the melt of o-phthalonitrile by stirring the mixture. The reaction between the components (25-30 min.) led to the formation of $EuPc_2$ (Figure 1). After completion of $EuPc_2$ synthesis, the temperature was increased to 350–400°C to distill off the excess o-phthalonitrile and other by-products of the reaction condensed in the top of the reactor. At the second stage, from the $EuPc_2$ molecules we obtained desirable pyrolyzate when the temperature in the reactor was fast increased to 850–900°C. In this process, a destruction of $EuPc_2$ molecules led to the formation of target product being finely dispersed carbon-metal powder. Previously, these substances we characterized by neutron scattering when determined their fine structure with a large volume fraction of pores (~ 50%) having very wide distribution by sizes ~ 10^0-10^2 nm [12,13]. Additionally, at the scales up to tens of microns some irregular "labyrinth structures" have been observed on the surface of the pyrolyzate particles being porous formations of carbon aggregates. This is illustrated in Figure 2 where Atomic Force Microscopy (AFM) pattern is presented for EuC_X (X~30–40).

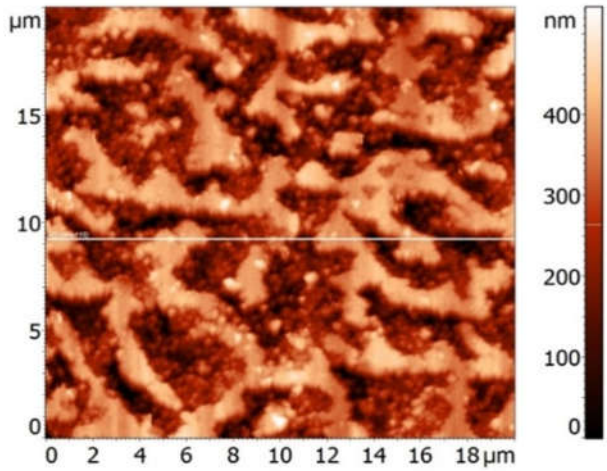

Figure 2. AFM image of EuC_X pyrolyzate surface.

Preprints (www.preprints.org) | NOT PEER-REVIEWED | Posted: 6 December 2022 doi:10.20944/preprints202212.0085.v1

In following X-ray wide angle scattering experiments (XRD), the pyrolyzate powder EuC_x showed completely amorphous structure discussed below. According to previous data [9], such carbon matrices retain metal atoms strongly. The immobilization of heavy elements in pyrolyzates was earlier tested by annealing up to 1600°C [9]. We used such temperature resistant precursor filled with pentaerythritol, $C(CH_2OH)_4$, to achieve a catalytic effect by diamond synthesis.

2.2. Synthesis and purification

For the synthesis of Eu-doped diamonds, we used the HPHT method optimized in the synthesis of microdiamond powders from different carbon precursors such as detonation nanodiamond [14], shock-wave polycrystalline diamonds [15] and carbon black [16] together with pentaerythritol or ethanol as the hydrocarbon sources.

In the experiments, EuC_x pyrolyzate powders mixed with pentaerythritol (50:50 wt.%) and packed into toroidal containers with graphite bushings were exposed to 11 seconds at high pressures and temperatures (7.5–8 GPa, 1800°C).

The sintered samples (cylinders) have been milled to prepare fine powders then mixed to prepare raw sample SEu1 containing diamond and other phases (graphite, aragonite, Eu-hydroxides) (Table 1). Following procedures included etching the samples (Seu2) in hydrochloric acid followed by the hydrostatic separation of graphite and diamond in bromoform, $CHBr_3$ (Seu3, Tab.1).

Table 1. Diamond containing samples with Eu.

Sample	Eu content	Purification, HCl	Treatment, $CHBr_3$	Diamond, wt.%	Graphite, wt.%
SEu1	5.7 wt. %	–	–	–	–
Seu2	88±5 ppm	+	–	52	48
Seu3	55±5 ppm	+	+	95	5

2.3. Methods

To study the powder samples, we have used the X-ray phase analysis (Rigaku Smart Lab III diffractometer, copper anode, Bragg-Brentano geometry, accelerating voltage 40 kV, current 30 A, Soller slits 2.5°, recording step 0.01°, speed 5°/min) and determined the composition of the crystalline phases by using the ICSD PDF2 database.

To determine the Eu concentration in diamonds, we applied radiometric X-ray analysis (XRA) [17], which reveals extremely small amounts (several ppm) of impurities in materials. This method, also known as XRF (X-ray fluorescence), is based on the measurement of secondary fluorescent X-rays emitted by a sample when it is excited by an X-ray source [18].

In the analysis of the samples with various Eu-contents we exploited different sources XRF@109Cd, XRF@241Am with moderate or high power (^{109}Cd radionuclide, activity of 0.36 GBq, quanta energy 22-25 keV, set of lines; ^{241}Am, activity of 80 GBq. quanta energy 59.5 keV). As the references, the Eu (III) oxides dissolved in water with 1 M HNO_3 served. The analysis has been performed on the X-ray spectrometer consisting of PGT1000-13 (GmbH) detector with the energy resolution of 200 eV for Kα radiation of Fe (6.4 keV) and ORTEC spectrometric system. The dependences of the radiation intensity I(E) on the energy of photons from probes (reference solutions, SEu1,2,3) were recorded, which showed spectra with Kα1, Kα2 lines for Eu atoms, the concentrations of which were estimated by the method [19].

Since the aim of the synthesis was to produce the luminescent diamonds due to Eu atoms in crystals, we tested them by the method of X-ray exited optical luminescence (XEOL) [20,21]. We studied the samples by irradiating them with X-rays (quantum energy 8 keV, wavelength λ = 0.154 nm) and detecting UV and visible radiation with the wavelengths λ = 380–900 nm. Through the system of slits, the radiation from the X-ray tube (1.5BSV29-Cu) entered the crystal monochromator separated quanta with the energy of

Preprints (www.preprints.org) | NOT PEER-REVIEWED | Posted: 6 December 2022 doi:10.20944/preprints202212.0085.v1

8.0 keV from a full spectrum. The slits and Soller collimator formed the X-ray beam 2x2 mm^2 (intensity of $1.5x10^6$ s^{-1}) directed to the sample surface. The AvaSpec ULS2048L optical spectrometer (diapason of 380–900 nm) provided a registration of luminescence photons induced by X-rays in the sample (finely dispersed powder) poured into a flat container, one of the walls of which was made of Mylar. For physicochemical analysis of samples, we used standard FTIR, Raman spectroscopy and SEM.

2.4. Simulation

At the final stage of the work, we adapted computer methods for modeling the growth of perfect nanocrystals and crystals with one embedded Eu atom (MM2 force field method, PerkinElmer Chem Office, Chem3D module) [22, 23].

3. Results and discussions

3.1. Structure of pyrolyzate

Before the diamond synthesis, we analyzed EuC_x pyrolyzate structure by XRD (20°C) which showed no crystalline reflects in the angular range 2θ = 10-133 deg. For amorphous powder irradiated with X-rays (wavelength λ = 0.154 nm) the scattering intensity $I(q)$ vs. scattering vector modulus $q = (4\pi/\lambda)\sin(\theta)$ exhibited only broad peaks at $q_1 \sim 50$ nm^{-1}, $q_2 \sim 30$ nm^{-1}, $q_3 \sim 17$ nm^{-1} (Figure 3). The first peak revealed the correlations at the distance $L_1 \sim 2\pi/q_1 \sim 0.13$ nm comparable to the bond length between carbon atoms, the second and third peaks displayed europium-carbon and other interatomic correlations with the lengths $L_2 \sim 2\pi/q_2 \sim 0.2$ nm, $L_3 \sim 2\pi/q_3 \sim 0.4$ nm.

To decode pyrolyzate structure, we reconstructed the spectrum of spatial correlations $G(R)$ from the data by indirect Fourier transform (ATSAS package) [24-26] (Figure 4). The profile of $G(R) = R^2\gamma(R)$ is defined by the pair correlation function $\gamma(R)$ for scattering centers (carbons, europium atoms, inhomogeneities in atomic packing) at the distances R = 0 -1.3 nm. The $G(R)$ distribution represents a wide peak with maximum position indicating the radii of detected metal–carbon particles, $R \sim 0.5$–0.7 nm, exceeding the size of the $EuPc_2$ molecule. Obviously, as a result of pyrolysis, the molecules united into globular particles, and each of them captured several Eu atoms in the carbon shell.

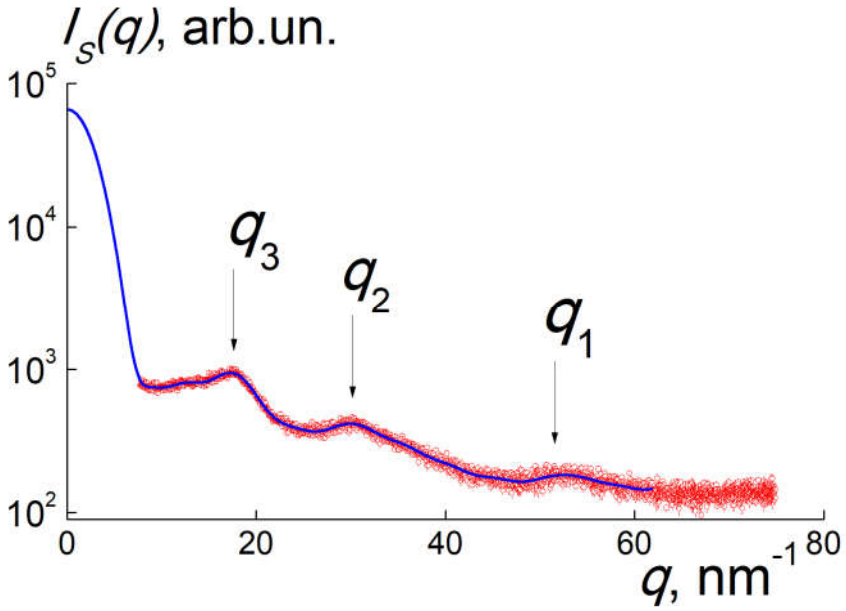

Figure 3. Intensity of X-ray scattering $I(q)$ on EuC_x pyrolyzate vs. scattering vector modulus. The positions of peaks ($q_{1\text{-}3}$) are marked. .

Preprints (www.preprints.org) | NOT PEER-REVIEWED | Posted: 6 December 2022 doi:10.20944/preprints202212.0085.v1

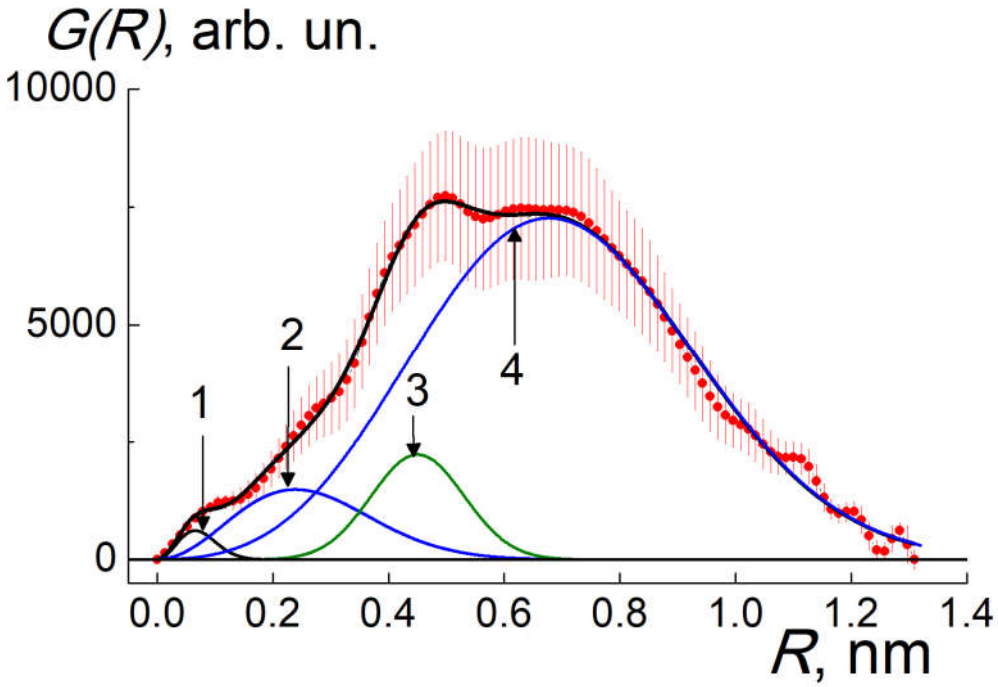

Figure 4. Distances distribution *G(R)* between scattering centers in EuC$_X$ pyrolyzate fitted with the function (1). Partial correlation functions (1-4) are plotted.

The core-shell model allowed describe the data in Figure 4 where the spectrum *G(R)* is a superposition of partial correlators for electron density within individual carbon atoms and small Eu clusters (G_1, G_2), the correlations between Eu and neighboring carbons (G_3), pair atomic correlations in the shell (G_4),

$$G(R) = \sum g_i G_i,\ i = 1,..4;\ G_{1,2} = R^2 \cdot \exp[-R^2/r_{1,2}^2],\ G_{3,4} = R^2 \cdot \exp[-(R-R_{3,4})^2/r_{3,4}^2]. \quad (1)$$

Here we neglected more extended cross-correlations of Eu atoms with carbon layers since the function (1) provided a satisfactory fit (Figure 4) with the coefficients g_i (amplitude factors). The other fitting parameters are the correlation lengths $r_{1,2}$ and $R_{3,4}$ with the dispersions $r_{3,4}$ (Table 2). Totally for globular structure described by the *G(R)* spectrum in Figure 4 we have found also the gyration radius $R_{GP} = 0.48 \pm 0.01$ nm which is close to the correlation length R_4. These lengths characterize a core-shell particle (Figure 5).

Table 2. Correlation lengths and dispersions in Eq.(1).

r_1, nm	r_2, nm	R_3, nm	r_3, nm	R_4, nm	r_4, nm
0.065 ±0.003	0.24 ±0.03	0.42 ±0.002	0.11 ±0.03	0.44 ±0.05	0.40±0.02

Preprints (www.preprints.org) | NOT PEER-REVIEWED | Posted: 6 December 2022 doi:10.20944/preprints202212.0085.v1

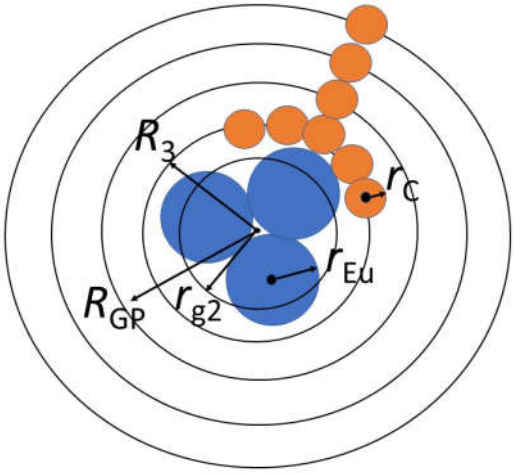

Figure 5. Globule with Eu-cluster and carbon shell (4 layers): r_C, r_{Eu} are atomic radii for carbon and Eu; r_{g2}, R_{GP} are gyration radii for Eu-cluster and globule, R_3 denotes a location of the carbon layer contacting with the Eu-cluster.

The parameters $r_{1,2} = (4/3)^{1/2} r_{g1,2}$ define the gyration radii $r_{g1,2}$ for electron density in carbon atoms and europium clusters. At longer scale, the R_3 is a characteristic distance between the Eu atoms in cluster and carbons in the layer adjacent to the cluster surface. The R_4 with the dispersion r_4 is the most probable length of correlations between carbons in the entire shell around the Eu cluster.

The r_1 gives the gyration radius of atomic electron shell $r_{g1} = (3/4)^{1/2} r_1 = 0.056 \pm 0.002$ nm, and in spherical approximation defines atomic geometric radius, $r_C = r_{g1}(5/3)^{1/2} = 0.073 \pm 0.003$ nm, corresponding to carbons ($r_C = 0.070$ nm) [8]. Similarly for Eu clusters, the r_2 determines their gyration and geometric radii, $r_{g2} = 0.21 \pm 0.03$ nm, $r_{CL} = r_{g2}(5/3)^{1/2} = 0.27 \pm 0.03$ nm. The radius r_{CL} is by 35% larger than that for single Eu atom, $r_{Eu} = 0.185$ nm [8]. Hence, a cluster integrates a number of Eu atoms $\nu \approx (r_{CL}/r_{Eu})^3 \approx 3$. In average a globule with Eu cluster involves $\nu \approx 3$ diphthalocyanines linked via free bonds of molecular ligands retained carbons but lost H, N atoms by pyrolysis. Such globules are aggregated into a metal-carbon matrix EuC_X (X =30–40) with residual nitrogen [8]. At the parameter $\nu \approx 3$ a single globule with Eu atoms includes a number of carbons, $n_t \approx 100$.

Inside a massive carbon shell, the Eu cluster with the radius $r_{CL} \sim 0.3$ nm is coordinated at characteristic distance $R_3 \sim 0.4$ nm with adjacent carbon layer of thickness $\delta_1 = 2r_3/\sqrt{2} = 0.16 \pm 0.04$ nm corresponding to carbon atom size. Cluster-shell contacts lead to complex formation with charge transfer from Eu to carbon atoms, that is confirmed in pyrolyzate powders by gamma-resonance spectroscopy, which revealed mostly the Eu^{3+} ions [27].

Longer pair atomic correlations in a globule consisting mainly of carbons are characterized by the distance R_4 with the dispersion r_4 being a measure of carbon shell thickness $\delta_t = 2r_4/\sqrt{2} = 0.56 \pm 0.03$ nm (~4 layers). Totally for such a globular structure described by the $G(R)$ spectrum (Fig.4) we have found the gyration radius $R_{GP} = 0.48 \pm 0.01$ nm which is close to the correlation length R_4.

The extended structural information we obtained by the integration of partial correlators. The integral $s_1 = \int G_1 dR \sim N_C Z_C^2$ is proportional to the quantity of carbons (N_C) in the sample, and their squared atomic number ($Z_C = 6$). For the Eu clusters, the integral $s_2 = \int G_2 dR \sim \nu N_{Eu} Z_{Eu}^2$ is defined by the quantity of Eu atoms (N_{Eu}), squared atomic ($Z_{Eu} = 63$) and aggregation (ν) numbers. The information on the cluster contact with neighboring carbons we obtained from the integral $s_3 = \int G_3 dR \sim 2 n_1 N_{Eu} Z_{Eu} Z_C$. At last, the integral for the whole carbon shell, $s_4 = \int G_4 dR \sim n_t N_C Z_C^2$, gives the number of constituent atoms (n_t).

Preprints (www.preprints.org) | NOT PEER-REVIEWED | Posted: 6 December 2022 doi:10.20944/preprints202212.0085.v1

Combining the equations $(\nu/n_t) = N_{Eu}/N_C$, $s_4/s_1 = n_t$, $s_4/s_2 = (N_C/N_{Eu})^2(Z_C/Z_{Eu})^2$, $s_3/s_1 = 2n_1(N_{Eu}/N_C)(Z_{Eu}/Z_C)$ we have found all the parameters: the number of carbons in a globule, $n_t = 88\pm23$; the C:Eu proportion, $N_C/N_{Eu} = 33\pm8$; the Eu aggregation number, $\nu = (N_{Eu}/N_C)n_t = 2.7\pm0.7$; the number of carbons near central Eu cluster, $n_1 = 15\pm7$. The parameters ν, n_t are quite close to the estimates obtained from the radii $r_{1,2,3}$, and C:Eu atomic proportion according to pyrolyzate stoichiometry, N_C/N_{Eu} =30-40 [8].

In previous studies [9-13], similar pyrolyzates serving for the immobilization of heavy nuclides exhibited an excellent chemical and structural stability by heating up to the temperatures 1200-1600°C. A substantial release of Ln atoms from such materials has been detected only above 1200°C [9]. Interested in the migration of Eu atoms, we estimated the corresponding activation energy E_{AEu} ~2.3 eV, which turned out to be three times lower than the energy of vacancy formation in graphite [28]. Thus, the E_{AEu} barrier is related to the diffusion of atoms from the pores that open in the matrix upon heating.

Such a heat-resistant precursor, which strongly retains heavy atoms, can serve as a favorable precursor for doping diamonds in the HPHT process. To intensify this process, we combined this precursor with a hydrocarbon substance (pentaerythritol), which has the catalytic properties found earlier in the synthesis of diamonds from carbon clusters of 40 nm in size [16]. We decided to saturate the pyrolyzate with pentaerythritol (Figure 6), which penetrates into the fine pores of the carbon matrix, where interaction with Eu atoms is possible by their release from the carbon frameworks during HPHT.

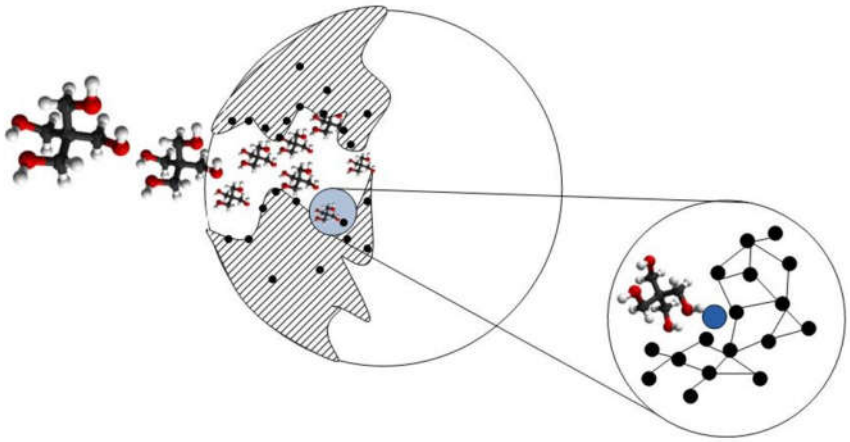

Figure 6. Pyrolyzate filled with pentaerythritol molecules which can interact with released Eu atoms at pores border by diamond synthesis.

In this way, we realized a favorable regime of transformation of pentaerythritol carbons into diamond with Eu-inclusions when the substance in pores is compressed at high temperatures. In the HPHT process, the Eu atoms firmly kept in globules of pyrolyzate became integrated into diamonds growing from the carbon in matrix. Both synergetic mechanisms promote in diamond formation with lanthanides that is discussed below.

3.2. X-ray diffraction and phase analysis

XRD patterns for the samples SEu1, SEu3 before purification and in final highly enriched state are shown in Figure 7. As we found, the raw sample SEu1 consists of graphite, diamond, aragonite ($CaCO_3$) and europium hydroxide, $Eu(OH)_3$. For these phases the mass contents are given in Figure 7. Aragonite contamination is caused by a partial incorporation of high-pressure chamber material into sintered sample. Some amount of graphite came from the graphite heater, the other part was formed as a result of crystallization of the carbon belonging to pyrolyzate and pentaerythritol under synthesis conditions. As

Preprints (www.preprints.org) | NOT PEER-REVIEWED | Posted: 6 December 2022 doi:10.20944/preprints202212.0085.v1

will be seen from the FTIR spectra, the diamond surface is covered with hydrogen. Therefore, it can be assumed with a high degree of probability that the synthesis occurs in a hydrogen-reducing medium. This suggests that under the synthesis conditions, europium was in the form of hydride, EuH_2, and turned into europium hydroxide, $Eu(OH)_3$, at room conditions after removal of temperature and pressure. Etching the SEu1 in hydrochloric acid resulted in the removal of aragonite and europium hydroxide. A significant part of graphite was removed by the hydrostatic separation of diamond from graphite in bromoform. As a result, we obtained the intermediate sample Seu2 with the proportion diamond:graphite = 52:48 wt. % (Table 1). The final well purified sample Seu3 contained 95 wt.% of diamond and 5 wt.% of graphite. Except of crystals, in diffraction we detected also nanographite inducing a wide halo in the region of 2θ = 17–38 deg. (Figure 7).

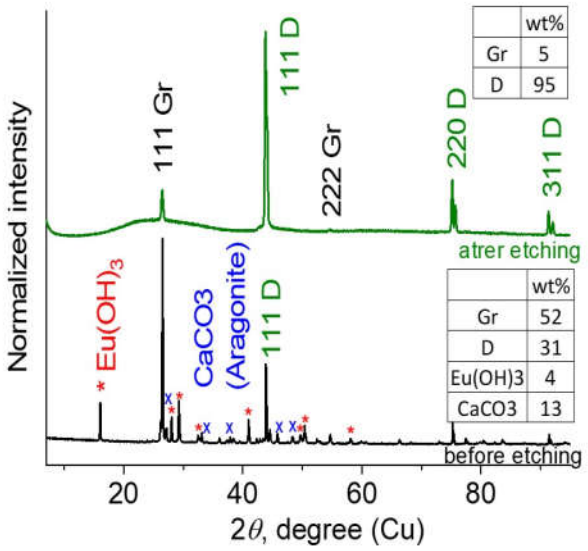

Figure 7. XRD patterns for the samples SEu1, Seu3. D – diamond, Gr – graphite. The weight of phases is shown in tables.

3.3. XRF, XEOL, TEM and Raman results

Primarily, in the raw sample SEu1, the XRF analysis showed the total Eu fraction of 5.7 wt. % (Table 1). According to the calculations, in the SEu1 only 3.9 wt.% of europium has entered the hydroxide phase. The residual part of 1.8 wt.% has retained in diamond and graphite. We confirmed the presence of Ln^{3+} ions in the sample SEu1 by XEOL. This is illustrated in Figure 8 where the peaks of Eu^{3+} ions luminescence are visible at wavelengths λ ~ 592; 616; 696 nm against a wide emission band (400-700 nm) arisen from the main components (diamond, graphite, aragonite) substantially contributing to the total intensity [29-32]. The characteristic Eu^{3+} emission bands should be attributed to the electron transitions $5D_0 \rightarrow {}^7F_{1,2,4}$ [33-35]. At the same time, the spectrum in Figure 8 did not show characteristic radiation from the ions Eu^{2+} (~500 nm) [36] which may present in minor quantities.

Preprints (www.preprints.org) | NOT PEER-REVIEWED | Posted: 6 December 2022 doi:10.20944/preprints202212.0085.v1

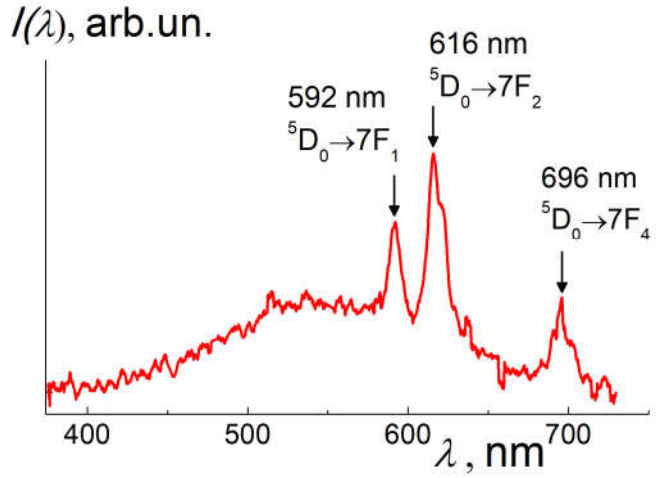

Figure 8. XEOL spectrum (excitation energy 8 keV) for the sample SEu1. Eu-peaks at characteristic wavelengths are marked, corresponding electron transitions are also shown.

The sample SEu2 purified, enriched with diamonds and tested by XRF@241Am has shown the substantial amounts of Eu, C_{Eu} = 88±5 ppm (Table 1). Finally, we have achieved a maximal segregation for diamonds, diamond:graphite = 95:5 wt.%, for the sample SEu3 (Figure 7, Table 1). These purified diamonds demonstrated a high quality judged by SEM showed good submicron(micron)-sized crystals with the smooth facets and a sharp cut (Figure 9).

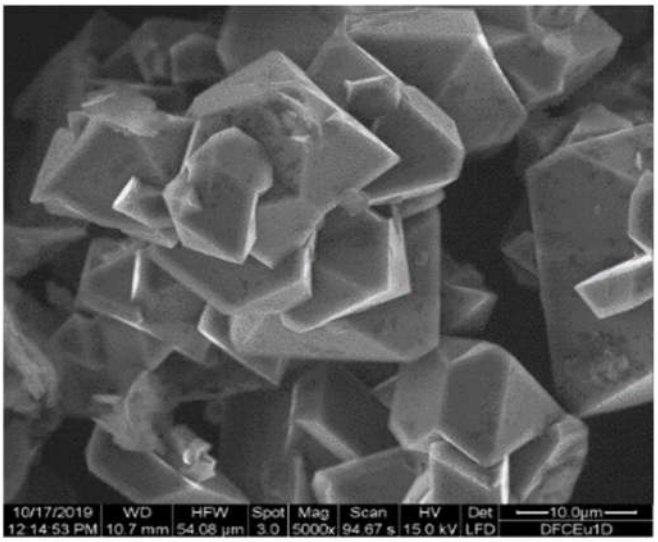

Figure 9. SEM image of purified diamond powder SEu3.

The Raman spectrum for these diamonds possessed a characteristic narrow peak (Figure 10) which obeys lorentzian $L(\kappa) \sim [(\kappa - \kappa_{max})^2 + \Gamma^2]^{-1}$ with the wavenumber at profile maximum κ_{max} = 1331.1 ±0.1 cm^{-1} and low width Γ = 2.19±0.05 cm^{-1} approaching to experimental resolution limit. The peak position being close to this one for bulk diamond (1332.5 cm^{-1}) [37,38] and very small linewidth both indicate monocrystals (>100 nm) in agreement with SEM pattern (Figure 9) and XRD which showed narrow diamond reflexes (Figure 7).

Preprints (www.preprints.org) | NOT PEER-REVIEWED | Posted: 6 December 2022 doi:10.20944/preprints202212.0085.v1

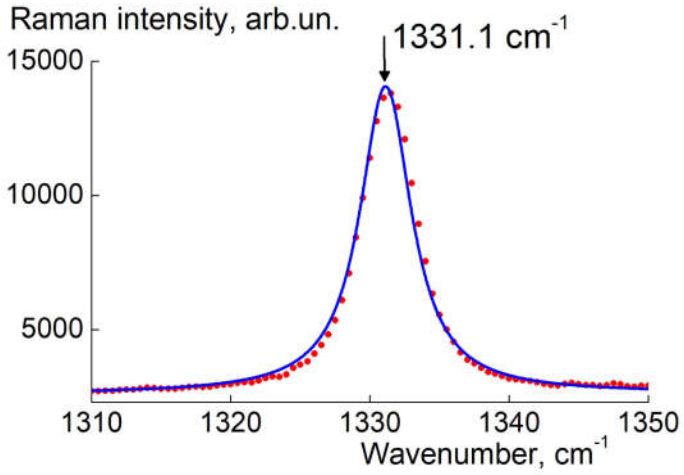

Figure 10. Raman spectrum for the sample SEu3 (dots). Lorentzian fitting (solid line).

By XRF@241Am we detected a characteristic X-ray fluorescence from Eu atoms in the powder SEu3 comparative to the reference solution with Eu(III) ions (Figure 11). Both the samples showed the emission with the intensities *I(E)* depending on photon energy with the peaks at E_{m1} =40.9 keV and E_{m2} =41.6 keV corresponding to Eu Kα2 and Eu Kα1 lines (Figure 11).

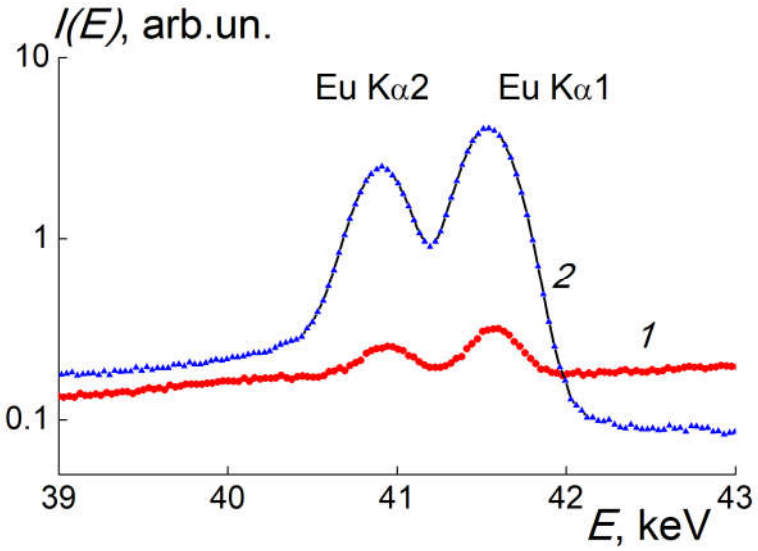

Figure 11. XRF@241Am spectra for the SEu3 (1) and reference sample (2). Eu Kα2 and Eu Kα1 lines are marked.

Following data processing with background subtraction and comparison of the integrals over emission peaks for the SEu3 and reference sample allowed us find the mass content of Eu in this sample, C_{Eu} = 55±5 ppm. The Eu atomic fraction C_{EuAt} = 4.2x10^{-4} % matches to an Eu atom per 2.3x10^{5} carbons (crystal fragment ~20 nm in size). The presence of Eu^{3+} ions in the sample we have confirmed by XEOL (Figure 12).

Preprints (www.preprints.org) | NOT PEER-REVIEWED | Posted: 6 December 2022 doi:10.20944/preprints202212.0085.v1

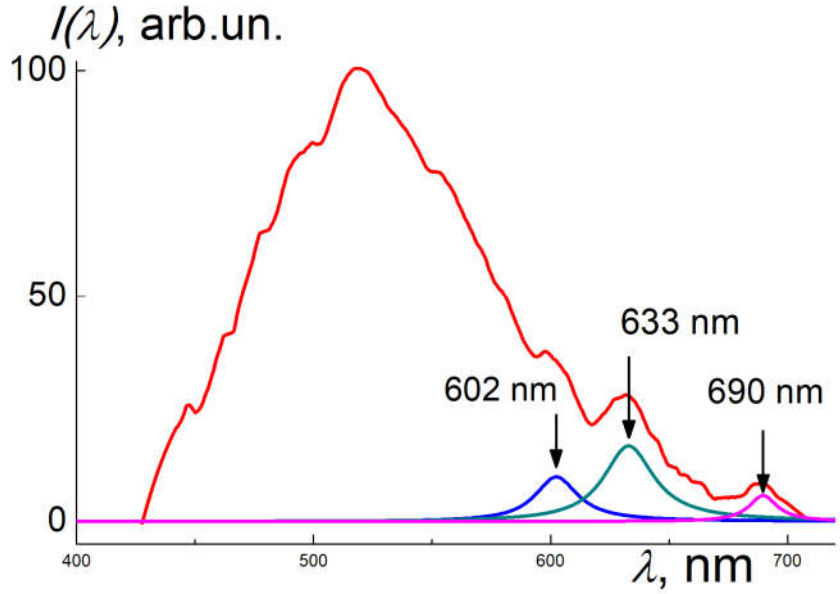

Figure 12. XEOL spectrum for the SEu3 sample showing Eu^{3+}characteristic bands. Lorentzian fitting is drawn with indication of maxima.

The luminescence spectrum (Figure 12) demonstrates a high emission in a wide band (450-600 nm) which is usually observed in diamonds due to electron-hole pairs generation by X-ray absorption and following pairs recombination on various lattice defects, including impurities and dislocations [29,30]. On the spectrum tail, we fitted the Eu specific peaks with lorentzians, $L(\kappa) = A_0[(\kappa - \kappa_{max})^2 + \Gamma^2]^{-1}$ and found their amplitudes (A_0), wavenumbers at the maxima (κ_{max}) and linewidths (Γ). All the lines at $\lambda_{max} = 1/\kappa_{max}$ = 602±1; 633±1; 690 ±1 nm have small widths, Γ/κ_{max} = 1.8±0.1; 2.0±0.1; 1.0±0.1 %.

The obtained fitting parameters defined the maximal peak intensities, A_0/κ_{max}^2, in the proportion 0.6:1:0.3 (Figure 12) which is close to the relationship between the intensities of Eu peaks in Fig.8 for raw sample SEu1, although maxima positions somewhat differ in these cases. Both spectra (Figure 8,12) represent the luminescence for the transitions $5D_0 \rightarrow {}^7F_{1,2,4}$ [33-35].

The evaluated spectral characteristics enabled us to find the ratio of summary intensity integrals over the Eu peaks to the integral over the band, $I_P/I_B \approx 2.5$ %. Surprisingly, even at extremely low quantity in the sample, the Eu atoms are explicitly visualized in the emission (Figure 12) due to X-ray high absorption by heavy atoms with atomic number ($Z_{Eu} = 63$) exceeding by an order in magnitude the number for carbons ($Z_C = 6$).

The linear absorption coefficient $\mu \sim \varrho Z^4/AE^3$ for X-rays in a substance is proportional to its density (ϱ) and strongly increases with the atomic number (Z) of constituent atoms while decreases with atomic weight (A) and quanta energy (E) [20].

In the sample SEu3 with doping degree C_{Eu}=55 ppm, the increase in the absorption coefficient is $\Delta\mu/\mu = (C_{Eu}A_C/A_{Eu})(Z_{Eu}/Z_C)^4 \approx 5$ % where A_C, A_{Eu} are atomic weights for carbon and Eu respectively. The ratio $I_P/I_B \approx 2.5$ % is half as much as $\Delta\mu/\mu$ due to nonradiative dissipation of absorbed energy.

The XRF and XEOL methods are in reasonable agreement and confirm the presence of Eu^{3+} ions in the sample S3 highly enriched with diamonds. On the other hand, in the case of XEOL one can suspect also other channels of luminescence induction due to various lattice defects attributed also to the impurities (N, O, H).

The FTIR spectrum (Figure 13) for the SEu3 showed different nitrogen impurities: neutral atoms at lattice sites (N0 or P1 defects), pairs of atoms in neighboring sites (2N, A-aggregates), ions N+(C+ defects) (Table 3).

Among them, A-aggregates are most common, and C+ defects are least of all present. In addition, the diamond surface is saturated with hydrogen. Despite of substantial

Preprints (www.preprints.org) | NOT PEER-REVIEWED | Posted: 6 December 2022 doi:10.20944/preprints202212.0085.v1

amount of nitrogen (471 ppm), the crystals possess a good quality (large sizes, smooth faces) according to the data of SEM and Raman spectroscopy (Figure 9,10).

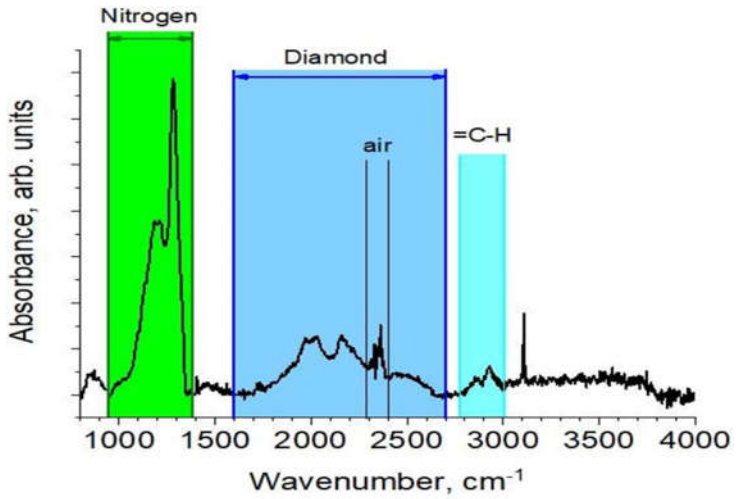

Figure 13. IR spectrum of the sample SEu5 wit Eu.

Table 3. Concentration of nitrogen defects according to FTIR data.

Wavenumber, cm^{-1}	Nitrogen defect type	Concentration, ppm
1132	Nº (C or P1)	156
1280	2N (A-aggregate)	287
1331	N^+ (C^+)	28
Sum		**471**

Detected by FTIR defects (Table 3) are practically invisible in XEOL experiments. The moderate amount of nitrogen (Table 3) it not appropriated for X-ray excitation of luminescence. Numerous defects preferably absorb in optical diapason and this effect is used to detect nitrogen in diamonds [39]. Only in rare cases, at low fraction of nitrogen, the XEOL spectra for diamonds have been registered [40]. Usually, the diamonds prepared by HPHT method demonstrate a wide smooth band of X-ray exited luminescence (400-600 nm) without any peculiarities owing to nitrogen defects [29].

Nevertheless, the total nitrogen content (C_N = 471 ppm, Table 3) exceeds the Eu amount by an order in magnitude, and numerous nitrogen defects may influence on the accommodation of Eu-atoms in diamond lattice. For example, complexes of metal atoms with nitrogen (Ni-N, Co-N) were found in natural diamonds as a result of the growth of crystals with dislocation-type defects in slip planes [41]. However, in our case the FTIR data did not reveal any complexing.

On the other hand, some of nitrogen defects are able to decrease lattice stresses when heavy atoms are embedded into diamond. The results of modeling [42,43] displayed a formation of B1-defects (4 nitrogen atoms associated with vacancy) which decrease the lattice energy comparative to perfect crystal. The effect is of (1-4) eV per one defect and varies as dependent on the amounts of nitrogen and hydrogen in crystal. Probably, a number of B1 defects surrounding the Eu atom in the lattice can compensate for the energy excess due to doping. But in the IR spectrum, we did not find any signs of such defects. On the whole, the role of nitrogen defects in the stabilization of Eu atoms in diamonds has not yet been elucidated.

Starting from the structure of pyrolyzate composed of carbon globules encapsulating Eu clusters, we believe partially their presence in diamonds which achieve doping degree much higher than that in synthetic or natural (carbonado) analogs [1,4,44]. Natural carbonado diamonds may contain the inclusions of hydrated rare-earth phosphates or metallic

Preprints (www.preprints.org) | NOT PEER-REVIEWED | Posted: 6 December 2022 doi:10.20944/preprints202212.0085.v1

phases (Fe, Fe-Ni, Ni-Pt, Si, Ti, Sn, Ag, Cu) when the size of inclusions is extended from few nanometers to much larger dimensions in the presence of aggregated nitrogen defects (N2V+, N2+, N3V, H1) indicating the synthesis of diamonds from the original hydrocarbon material [4,44,45]. The studies of natural diamonds with rare earth elements and metallic phases showed a fundamental possibility of artificial synthesis of such diamonds at high pressures and temperatures from hydrocarbon materials.

In our diamonds we have got a record high Eu amount, C_{EuD} = 51±5 ppm, in the limit of the samples free of graphite and determined also the Eu content in graphite, C_{EuG} = 128±5 ppm. To clarify the subtle features of diamond modification with Eu, we simulated the growth of single crystals with defects including metal ion and vacancy, (Eu^{3+}–V), and built also an ideal crystal (3d model, 528 atoms, the distance between the extreme atoms is ~1.8 nm) as a reference using the MM2 force field method [22,23].

Simulation of the formation of nanocrystals by sequential stacking of atoms in a growing structure in the cases of an ideal crystal and a crystal with one Eu atom gave a positive energy difference between the data for defective and perfect crystals. The resulting energy costs E_{Eu} = 5.8 eV for the formation of a defect with Eu and a vacancy are higher, but comparable to the binding energy of atoms in bulk diamond (~2.5 eV) [46].

Previously, the authors of [1] simulated the formation of the (Eu^{3+}-V) complex inside a small lattice fragment (64 atoms) and determined the energy of a diamond fragment with such a defect, E_{EuD} ≈ 13.8 eV [1]. For such a defective crystal fragment, we obtained the energy E_{EuD} ≈ 15.5 eV by eliminating the contribution of external carbon atoms around the fragment. Both quantities are comparable, although the simulation procedures were different and an exact match cannot be expected.

During the HPHT process at the temperature T ~ 2100 K each a carbon atom in pyrolyzate gets a substantial kinetic energy, $E_1 \sim k_B T$ ~ 0.2 eV, which partially is expended for Eu-defects formation. To create a defect with the energy cost E_{Eu} = 5.8 eV, it takes a participation of ~ 30 carbons around a heavy atom. Hypothetically, in diamonds may exist the globules composed of Eu-clusters (~3 atoms) with massive shells of ~ 90 carbons rearranged to cover energy cost for such a defect stabilization in the lattice.

Finally, we have to note, that a direct observation and structural analysis of Eu-defects are very difficult due to small concentrations of these inclusions and did not carry out in this work, which unambiguously showed really effective way of Eu atoms integration into the diamond lattice. Until now, this remains an open question in theory and experiment [47-50].

4. Conclusions

The synthesis of diamonds using a heat-resistant ultraporous precursors, diphthalocyanine pyrolyzates, made it possible to obtain diamonds doped with Eu atoms up to the concentrations C_{EuD} = 51±5 ppm almost two orders of magnitude higher than those in natural diamonds (carbonado) and synthetic analogues.

The developed precise technique of X-ray fluorescence measurements allowed us determine reliably the Eu contents in the samples upon their activation. The results are consistent with the measurements showed a characteristic luminescence from Eu^{3+} ions in diamonds exposed by X-rays.

The incorporation of Eu atoms into diamond lattice was highly facilitated by metal-carbon precursor composed of specific globular structures with small clusters of heavy atoms inside massive carbon shells kept them during HPHT synthesis.

The proposed methodology seems to be promising for the development of diamond doping technologies using special type nano-precursors.

Funding: This research was funded by the Russian Foundation for Basic Researches, grant number 18-29-19008, partially by Kurchatov Institute according to the state assignment for the theme "2.4. Carbon based nanomaterials" and by Governor fellowship of Leningrad district personally for V.T.Lebedev.

 doi:10.20944/preprints202212.0085.v1

Acknowledgment: Authors are very grateful to engineers I.N.Ivanova and L.I.Lisovskaya, Drs. V.I.Tikhonov and V.Yu. Bairamukhov for technical assistance.

Conflict of Interests: The authors declare no conflicts of interest.

Author Contributions: Conceptualization, Lebedev V.T. and Vul A.Ya.; HPHT synthesis and purification, SEM, XRD, FTIR, Shakhov F.M.; Software and computer simulations, Zakharov; XRF measurements and analysis, Zinoviev V.G.; Raman spectroscopy, Orlova V.A.; XEOL experiments, Fomin E.V.; Writing – Original Draft Preparation, Lebedev V.T.; Editing, Shakhov F.M.

References

1. Magyar, A.; Hu, W.; Shanley, T.; Flatter, M.E.; Hu, E.; Aharonovich, I. Synthesis of luminescent europium defects in diamond. *Nat. Commun.* **2014**, *5*, 1–6. doi.org/10.1038/ncomms4523
2. Sotoma, S.; Hsieh, F.J. ; Chang, H.-C. Biohybrid fluorescent nanodiamonds as dual-contrast markers for light and electron microscopies. *J. Chin. Chem. Soc.* **2018**, *65*, 1136–1146. doi.org/10.1002/jccs.201800157D
3. Kidalov, S.V.; Zamoryanskaya, M.V.; Kravez, V.A.; Sharonova, L.V.; Shakhov, F.M.; Yudina, E.V.; Artamonova, T.O., Khodorkovskii, M.A.; Vul, A.Ya. Photo- and cathodoluminescence spectra of diamond single crystals formed by sintering of detonation nanodiamond. *Nanosyst: Phys, Chem, Math.* **2019**, *10*, 12–17. doi.org/10.17586/2220-8054-2019-10-1-12-17
4. Shibata, K.; Kamioka, H.; Kaminsky, F.V.; Koptil, V.I.; Svisero, D.P. Rare earth element patterns of carbonado and yakutite: evidence for their crustal origin. *Mineral. Mag*. **1993**, *57*, 607–611. doi.org/10.1180/minmag.1993.057.389.05
5. Ekimov, E.A.; Zibrov, I.P.; Malykhin, S.A.; Khmel'nitskii, R.A.; Vlasov, I.I. Luminescence properties of diamond prepared in the presence of rare-earth elements. *Inorg. Mater*. **2017**, 53, 809–815. doi.org/10.1134/S0020168517080039
6. Malashkevich, G.E.; Lapina, V.A.; Semkova, G.I.; Pershukevich, P.P.; Shevchenko, G.P. Luminescence of Eu 3+ ions in ultradisperse diamond powders. *JETP Letters* **2003**, *77*, 291–294. doi.org/10.1134/1.1577759
7. Chen, Xiaofeng; Song, J.; Chen, Xiaoyuan; Yang, H. X-ray-activated nanosystems for theranostic applications. *Chem. Soc. Rev*. **2019**, *48*, 3073–3101. doi.org/10.1039/C8CS00921J
8. WebElements. Available online: https://www.webelements.com, accessed October 2022. The periodic table on the WWW [www.webelements.com]. Copyright 1993-2022 Mark Winter. The University of Sheffield and WebElements Ltd, UK.
9. Tikhonov,V.I.; Kapustin,V.K.; Lebedev,V.T.; Sovestnov, A.E.; Bairamukov,V.Yu.; Mishin, K.Ya. A carbon composite based on pyrolyzed diphthalocyanines for immobilization of high-level waste from nuclear industry. *Radiochemistry* **2016**, *58*, 545–555. doi.org/10.1134/S1066362216050167
10. Lebedev, V.T., Sovestnov, A.E.; Tikhonov V.I.; Chernenkov, Yu.P.. Structure of the amorphous phase of pyrolisates of lanthanum diphthalocyanine according to X-Ray scattering data. *J. Surf. Investig.: X-ray Synchrotron Neutron Tech.* **2017**,*11*, 38–48. doi.org/10.1134/S1027451017010165
11. Moskalev, P.N.; Sibilev, A.I. Action of gaseous ammonia and water on neodymium diphthalocyanine. *Russ. Chem. Bull.* **1998**, *47*,1406–1408. doi.org/10.1007/BF02495579
12. Lebedev, V.M.; Lebedev, V.T.; Orlova, D.N.; Sovestnov, A.E.; Tikhonov,V.I. Effect of annealing temperature on the structure of pyrolysates of diphthalocyanines of rare-earth elements: neutron research. *J. Surf. Investig.: X-ray Synchrotron Neutron Tech.* **2014**, *8*, 1002–1009. doi.org/10.1134/s1027451014050334
13. Lebedev, V.M.; Lebedev, V.T.; Orlova., D.N.; Tikhonov, V.I. Study of the structure of carbon matrices for radionuclide encapsulation by small-angle neutron scattering. *J. Surf. Investig.: X-ray Synchrotron Neutron Tech.* **2014**, *8*, 411–417. doi.org/10.1134/S1027451014030094

14. Shakhov, F. M.; Abyzov, A. M.; Takai, K. Boron doped diamond synthesized from detonation nanodiamond in a C-O-H fluid at high pressure and high temperature. *J. Solid State Chem.* **2017**, 256, 72-92.
15. Osipov, V.Yu.; Shakhov, F.M.; Bogdanov, K.V.; Takai, K.; Hayashi,T.; Treussart, F.; Baldycheva, A.; Hogan B.T.; Jentgens, C. High-quality green-emitting nanodiamonds fabricated by HPHT sintering of polycrystalline shockwave diamonds. *Nanoscale Res. Lett*. **2020**, *15*, 209 (1-13). doi.org/10.1186/s11671-020-03433-7.
16. Oshima, R.; Iizuka, K.; Vul, A.Ya.; Shakhov, F.M. Single crystal diamond particles formed by the reaction of carbon black and solid alcohol under high-pressure and high-temperature. *J. Cryst. Growth.* **2022**, *587*, 126646. https://doi.org/10.1016/j.jcrysgro.2022.126646.
17. Mukhamedshina, N.M.; Mirsagatova, A.A.; Zinov'ev, V.G. Determination of ZnSe(Te) stoichiometry and dopant content by X-ray analysis. *J. Radioanalytical and Nuclear Chem.* **2005**, *264(1)*, 97–100.
18. Streli, C. ; Wobrauschek, P. ; Kregsamer, P. X-ray Fluorescence Spectroscopy, Applications. In *Encyclopedia of Spectroscopy and Spectrometry*, Lindon, J., Tranter, G., Holmes, J. Eds.; Academia Press Ltd: London, UK, 2000; pp. 2478-2487. DOI: 10.1006/rwsp.2000.0337.
19. Zinovyev, V. G.; Lebedev, V.T.; Mitropolsky, I.A.; Shulyak G. I.; Sushkov, P. A.; Tyukavina T. M.; Okunev, I.S.; Ershov, K.V.; Balin. D.V. Determination of lanthanides and 3d metals in endovetallofullerenes water solutions by X-ray fluorescence spectrometry. *Intern. Sci. J. "Eurasian Union of Scientists" (EUS)* **2019**, *8(65)*, 40-44. doi:10.31618/ESU.2413-9335.2019.4.65.271.
20. Bunker, G.; Ed.; *Introduction to XAFS, A Practical Guide to X-ray Absorption Fine Structure Spectroscopy*, Cambridge Press: Cambridge, UK, 2010.
21. Taylor, R. The development of X-ray Excited Optical Luminescence (XEOL) spectroscopic techniques for mineralogical and petrological applications. Ph. Dr., University of St. Andrews. UK, Research@StAndrews:FullTextat:http://research-repository.st-andrews.ac.uk/, 2013.
22. Allinger, N.L. MM2 Force Field. *J. Am. Chem. Soc.* **1977**, *99*, 8127-8134.
23. Laqua, G. ; Musso, H. ; Boland, W. ; Ahlrichs, R. Force field calculations (MM2) of carbon lattices. *J. Am. Chem. Soc*. **1990**, *112(20)*, 7391–7392.
24. Svergun, D.I. Determination of the regularization parameter in indirect-transform methods using perceptual criteria. *J. Appl. Cryst.* **1992**, 25, 495–503. doi.org/10.1107/S0021889892001663.
25. Feigin, L. A.; Svergun, D. I. *Structure Analysis by Small- Angle X-ray and Neutron Scattering*; Plenum Press: New York, NY, USA, 1987.
26. Manalastas-Cantos, K.; Konarev, P. V.; Hajizadeh, N. R.; Kikhney, A. G.; Petoukhov, M. V.; Molodenskiy, D. S.; Panjkovich, A.; Mertens, H. D. T.; Gruzinov, A.; Borges, C.; et al. ATSAS 3.0: Expanded Functionality and New Tools for Small-angle Scattering Data Analysis. *J. Appl. Cryst.* 2021, *54(1)*, 343–355. doi:10.1107/ s1600576720013412.
27. Kozlov,V.S.; Semenov, V.G.; Bayramukov, V.Yu. Transmission electron microscopy and Mössbauer spectroscopy of europium diphthalocyanine. *Communication of NRC KI – PNPI*. **2022**, *3070*, 1-16.
28. Li, L.; Reich, S.; Robertson, J. Defect energies of graphite: Density-functional calculations. *Phys. Rev.* **2005**, *B72*, 184109.
29. Osadchy, A. V.; Vlasov, I. I.; Kudryavtsev, O. S.; Sedov, V. S.; Ralchenko, V. G.; Batygov, S. H.; Savin, V. V.; Ershov, P. A.; Chaika, V. A.; Narikovich, A. S.; Konov, V. I. Luminescent diamond window of the sandwich type for X-ray visualization. *Appl. Phys. A* **2018,** *124*, 807 (1-5). doi.org/10.1007/s00339-018-2230-0.
30. Mironov,V.P.; Emelyanova, A. S.; Shabalin, S. A.; Bubyr, E. V.; Kazakov, L. V.; Martynovich, E. F. X-ray luminescence in diamonds and its application in industry. XVIII International Conference on Luminescence and Laser Physics (LLPH), 5-10 July 2021, Irkutsk. Russia. *AIP Conf. Proc.* **2021**, *2392*, 020010. doi.org/10.1063/5.0061972.

31. Toffolo, M. B.; Ricci, G.; Caneve, L.; Kaplan-Ashiri, I. Luminescence reveals variations in local structural order of calcium carbonate polymorphs formed by different mechanisms. *Sci. Rep.* **2019**, *9*, 16170. doi.org/10.1038/s41598-019-52587-7. www.nature.com/scientificreports.
32. Chiou, J. W.; Ray, S. C.; Peng S. I.; Chuang, C. H.; Wang, B. Y.; H. M. Tsai, C. W. Pao, H.-J. Lin, Y. C. Shao, Y. F. Wang, S. C. Chen, W. F. Pong, Y. C. Yeh, C. W. Chen, L.-C. Chen, K.-H. Chen, M.-H. Tsai, A. Kumar, A. Ganguly, P. Papakonstantinou, H. Yamane, N. Kosugi, T. Regier, L. Liu,T. K. Sham. Nitrogen-Functionalized Graphene Nanoflakes (GNFs:N): Tunable Photoluminescence and Electronic Structures. *J. Phys. Chem.. C* **2012**, *116(30),* 16251-16258. DOI: 10.1021/jp303465u.
33. Zhigunov, D. M. ; Abdullaev O. R. ; Ivannikov, P. V. ; Shishonok, E. M. ; Urbanovich, S. I. ; Kashkarov, P. K. Photo- and cathodoluminescence of cubic boron nitride micropowders activated by Tm, Tb, and Eu rare-earth ions. *Moscow Univer. Phys. Bull.* **2016**, *71*, 97–104. doi: 10.3103/S0027134916010185.
34. Kaplyanskiĭ, A. A. ; Kulinkin, A. B. ; Kutsenko A. B. ; Feofilov, S. P. ; Zakharchenya, R. I. ; Vasilevskaya, T. N. Optical spectra of triply-charged rare-earth ions in polycrystalline corundum. *Phys. of Solid State* **1998**, *40*, 1310–1316.
35. Smagin, V. P. ; Khudyakov, A. P. ; Biryukov, A. A. Luminescence of Eu^{3+} Ions in a Matrix of a Fluorinated Yttrium–Aluminum Composition. *Phys. of Solid State* **2020**, *62*, 325–331. DOI: 10.1134/S1063783420020195
36. dos S. Rezende, M. V. ; Montes P. J. R. ; Andrade, A. B. ; Macedo, Z. S. ; Valerio, M. E. G. Mechanism of X-ray excited optical luminescence (XEOL) in europium doped $BaAl_2O_4$ phosphor. *Phys. Chem. Chem. Phys*. **2016**,18(26),17646-17654
37. Vlasov, I.I.; Shenderova, O.A. Raman and Photoluminescence Spectroscopy of Detonation Nanodiamonds in Detonation nanodiamonds. Science and applications, Vul, A.Ya., Shenderova O.A., Eds.; Pan Stanford Publishing Pte. Ltd.: Danvers, USA, 2014. Ch.5. pp. 121-149.
38. Koniakhin, S.V.; Utesov, O. I.; Terterov I. N.; Siklitskaya, A. V.; Yashenkin, A. G.; Solnyshkov, D. Raman Spectra of Crystalline Nanoparticles: Replacement for the Phonon *Confinement Model. J. Phys. Chem. C* **2018**, *122*, 19219–19229. doi: 10.1021/acs.jpcc.8b05415.
39. Lyutoev, V.P.; Glukhov, Yu.V.; Schanov, M.F. X-ray luminescent method for determining nitrogen defects in diamonds. Patent RU 2 215 285 C1. Start date of the patent 13.03. 2002. Published 27.10.2003.
40. Isaenko, S. I. X-ray stimulated luminescence of nitrogen defects in natural diamonds/ Structure, substance, history of the lithosphere of the Timan-Severoural segment. In Information materials of the 9th scientific conference of the Institute of Geology of the Komi Scientific Center of the Ural Branch of the Russian Academy of Sciences, Syktyvkar, Russia, 7-8 December, 2000. Geoprint: Syktyvkar, 2000; pp. 56-58.
41. Tretyakova,L.I.; Lyukhin, A.M. Impurity, defect centers and inclusions in natural diamonds are characteristics of the cosmogenic-impact-metamorphogenic-metasomatic history of their genesis. *Ural Geological Journal* **2017**, *3(117),* 43-74.
42. Miyazaki, T. ; Okushi, H. ; Uda, T. Shallow donor state due to nitrogen-hydrogen complex in diamond. *Physical Review Letters* **2002**, 88, 066402. doi: 10.1103/PhysRevLett.88.066402.
43. Zheng, Y.; Li, C.; Liu, J.; Wei, J.; Ye H. Diamond with Nitrogen: States, Control and Applications. *Functional Diamond* **2021**, *1(1),* 63-82. doi: 10.1080/26941112.2021.1877021.
44. Heaney, P. J.; Vicenzi, E. P.; De, S. Strange Diamonds: The Mysterious Origins of Carbonado and Framesite. *Elements* **2005**, *1*, 85-89.
45. Nadolinny, V.A.; Shatsky, V.S.; Sobolev, N.V.; Twitchen, D.J.; Yuryeva, O.P.; Vasilevsky I.A.; Lebedev, V.N. Observation and interpretation of paramagnetic defects in Brazilian and Central African carbonados. *American mineralogist* **2003**, *88(1),* 11-17. doi.org/10.2138/am-2003-0102.
46. Vul, A.Ya.; Shenderova, O.A. Carbon at the Nanoscale, in Detonation nanodiamonds. Science and applications, Vul, A.Ya., Shenderova, O.A. (Eds.). Pan Stanford Publishing Pte. Ltd.: Danvers. USA, 2014; ch.5, pp.1-35.

47. Palyanov, Y. N.; Borzdov, Y. M. ; Kupriyanov, I. N. ; Khohkhryakov A. F.; Nechaev, D. V. Rare-earth metal catalysts for high-pressure synthesis of rare diamonds. *Scientific Reports* **2021**, *11*, 8421. doi.org/10.1038/s41598-021-88038-5
48. Vanpoucke, D. E. P.; Nicley,S. S.; Raymakers J.; Maes, W.; Haenen K. Can Europium Atoms form Luminescent Centres in Diamond: A combined Theoretical-Experimental Study. *Diamond and Related Materials* **2019**, *94*, 233-241. doi:10.1016/j.diamond.2019.02.024.
49. Sedov,V.; Kouznetsov, S.; Martyanov, A.; Proydakova, V.; Ralchenko, V.; Khomich, A.; Voronov, V.l Batygov, S.; Kamenskikh, I.; Spassky, D.; Savin S.; Fedorov, P. Diamond−Rare Earth Composites with Embedded NaGdF4:Eu Nanoparticles as Robust Photo- and X-ray-Luminescent Materials for Radiation Monitoring Screens. *ACS Appl. Nano Mater*. **2020**, *3*, 1324−1331. doi.org/10.1021/acsanm.9b02175
50. Yudina, E.B.; Aleksenskii, A.E.; Bogdanov, S.A.; Bukalov, S.S.; Leites, L.A.; Radishev, D.B.; Vikharev, A.L.; Vul', A.Y. CVD Nanocrystalline Diamond Film Doped with Eu. *Materials* **2022**, *15*, 5788. doi.org/10.3390/ ma15165788